Spectral lines of OH radicals and Na atoms in sonoluminescence

Yu An[1,2] and Chaohui Li[1]
[1]*Department of Physics, Tsinghua University, Beijing 100084, China*
[2]*Institute of Acoustics, Chinese Academy of Science, Beijing 100080, China*
(Received 25 August 2008; published 27 October 2008)

With the equations of fluid mechanics, the proper boundary conditions, and the gas properties, we simulate the processes of single-bubble sonoluminescence. The calculation demonstrates the process of the evolution of the radiation energy spectrum with time for bright sonoluminescing bubbles, which clearly shows how the prominence of the OH line near 310 nm gradually merges into the continuous spectral background as the radiation power increases and finally disappears in the spectrum. For the dim bubble, the spectral line of OH radicals or the sodium line near 589 nm is prominent on the spectrum.

DOI: 10.1103/PhysRevE.78.046313 PACS number(s): 78.60.Mq, 33.70.Jg

INTRODUCTION

It has long been known that in an intense acoustic field in water, a cavitation occurs, and those cavitation bubbles usually glow in the darkness [1], a phenomenon called multibubble sonoluminescence (MBSL). When the water is degassed, the frequency and the amplitude of the driving acoustic wave properly adjusted, a stable single-bubble sonoluminescence (SBSL) may be observed [2,3]. There are a lot of interesting issues related to SBSL [4], among which the mechanism of SBSL is the most puzzling one. Once there was a widespread viewpoint that the mechanism of SBSL was different from that of MBSL, and the evidence was that the line of OH radicals near 310 nm and the sodium line near 589 nm were absent in the SBSL spectrum, while both emerged in the MBSL spectrum [5]. However, a few years later, the OH line near 310 nm was observed in the case of an unstable SBSL [6], and recently both the OH line and the sodium line were observed in the case of a stable but dim SBSL under lower driving acoustic pressure [7]. These experiments suggest the similarities between MBSL and dim SBSL. In the diffusive equilibrium diagram [8], those unstable SBSL bubbles are at the area with lower driving acoustic pressure. Usually, with lower driving acoustic pressure, the maximum temperature inside the bubble is lower. Since the presence of the line spectrum points to lower temperatures [9], it seems that those individual bubbles of MBSL may be similar to those dim SBSL bubbles corresponding to the lower maximum temperatures. These important arguments are just directly speculated from the experiments and need support from detailed calculations. With calculations, it is possible to figure out how and when the spectral lines merge into the continuous background of SBSL spectrum, etc.

Recently, we developed a calculation model of SBSL [10], where the equations of the fluid mechanics of two gas components, inert gas [11] and water vapor, are employed to describe gas dynamics inside the bubble; the mass action law [12] is applied to evaluate the production of chemical reaction and the ionization; at the boundary of the bubble, the phase transition of vapor and heat exchange are considered; electron-neutral atom bremsstrahlung [13], electron-ion bremsstrahlung and recombination radiation [14], and the radiative attachment of electrons to atoms and molecules [15,16], which contribute to the continuous spectrum, are included in the light emission calculation. The present calculation covers the additional computation of the OH line near 310 nm, as well as the spectral band of vibration and rotation, the sodium line near 589 nm, and their broadening caused by the collision between molecules or resonance. Through the computational research of SBSL, we may obtain detailed information inside the SBSL bubble, come to understand what conditions make the spectral lines appear and disappear, and further estimate the maximum temperature inside the sonoluminescing bubble.

COMPUTATION MODEL AND FORMULAS

The calculation formulas are almost similar to those deduced in Ref. [10], with a few others listed below. One difference is the Rayleigh-Plesset (RP) equation. The different forms of the RP equation make a small difference to the bubble motions, but a relatively large difference to the gas dynamics results [17]. Yet this problem is not solved, and we will not repeat the discussion here. We just adopt the simplest form of the RP equation [18] with slight improvement:

$$R\ddot{R} + \frac{3}{2}\dot{R}^2 = \frac{1}{\rho_l}[p_l - p_\infty - p_s(t+t_R)] + \frac{t_R}{\rho_l}\dot{p}_l, \tag{1}$$

where t is the time, $R(t)$ the radius of the bubble, p_∞ the ambient pressure, $p_s(t) = -p_a \sin(\omega t)$ the driving acoustic pressure, $t_R \equiv \frac{R}{c_l}$, c_l the sound speed in the liquid at the ambient temperature and under the pressure of 1 atm, $p_l = p_g(R,t) - \frac{4\eta\dot{R}}{R} - \frac{2\sigma}{R}$ the pressure on the liquid side of the bubble wall, $p_g(R,t)$ the pressure on the gas side of the bubble wall, η the dynamic viscosity, and σ the surface tension coefficient of the liquid. The improvement is that those ρ_l and c_l are not constant anymore, and they need to be calculated with the Tait equation, an equation of state of water:

$$\frac{p_l + B}{p_\infty + B} = \left(\frac{\rho_l}{\rho_{l\infty}}\right)^n, \tag{2}$$

where B and n are constants slightly dependent on temperature and $\rho_{l\infty}$ the ambient liquid density. To some extent,

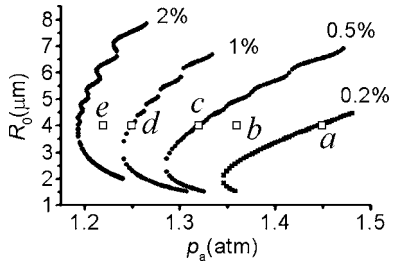

FIG. 1. Diffusive equilibrium curves in R_0-p_a parameter space for five different gas concentrations in water—namely, 0.2%, 0.5%, 1%, and 2%, respectively—corresponding to a driving acoustic wave frequency of 34 kHz.

this improvement embodies the effect of the liquid compressibility.

Another formula slightly different from that in Ref. [10] is the radiation power. In opaque media, the more appropriate formula of the radiation power from a SBSL bubble per wavelength interval at wavelength λ should be

$$P(\lambda,t) = 8\pi^2 \int_0^R \int_{-1}^1 \kappa_\lambda(r) P_\lambda^{\mathrm{Pl}}(r) \times \exp\left(-\int_{rx}^{\sqrt{R^2-r^2(1-x^2)}} \kappa_\lambda ds\right) r^2 dr\, dx, \tag{3}$$

where r is the radial coordinate, P_λ^{Pl} the Planck radiation intensity, κ_λ the absorption coefficient, and λ the wavelength. The contributions of continuous spectral parts to κ_λ can be calculated with those formulas exactly the same as in Ref. [10]. For the line spectrum,

$$\kappa_\lambda = \frac{\lambda^5}{2hc^2}(e^{hc/\lambda kT} - 1) P_\lambda, \tag{4}$$

where P_λ represents the radiation power per unit volume per unit wavelength interval of the line spectrum.

For line spectra of SBSL, the transition $A^2\Sigma^+ \rightarrow X^2\Pi_i$ of the OH radical may be interesting. Since there are considerable vibrational and rotational states in each electronic state, the line spectrum extends to a band. Considering a transition from the excited state OH* $(A^2\Sigma^+)$ with vibrational and rotational quantum number v and J, respectively, to the OH $(X^2\Pi_i)$ state with v' and J', the excited state may be obtained through the reaction [19] of $\mathrm{O+H+}M \rightarrow \mathrm{OH^*+}M$ (M is the third particle). Then, the power of radiation per unit volume of that transition [20] can be calculated as

$$P_{vJ,v'J'} = k_r n_O n_H n_M f \frac{(2J+1)e^{-E(v,J)/kT}}{Q_{v,J}} A_{\mathrm{vib}}^{vv'} A_{\mathrm{rot}}^{JJ'} h\nu_{vJ,v'J'}, \tag{5}$$

where k_r is the coefficient of the reaction rate, n_i the particle number density of i species, f the factor to estimate the quenching of the radiation by collisions with other particles [15,21], Q_{vJ} the partition function, and $E(v,J)$ the energy of the vibrational and the rotational state (v,J). The vibrational part $A_{\mathrm{vib}}^{vv'}$ can be found in Ref. [22], and the rotational part $A_{\mathrm{rot}}^{JJ'}$ can be evaluated by the Hönl-London formulas [20]. $h\nu_{vJ,v'J'}$ is the photon energy.

Since inside the sonoluminescing bubble there is high pressure, high density, and high temperature, the optical line intensity distribution may be of the Lorentz profile [23], and we obtain the radiation power of OH molecules per unit volume per unit wavelength interval given by

$$P_\lambda d\lambda = \sum_{vv',JJ'} P_{vJ,v'J'} g_{vJ,v'J'}\left(\nu = \frac{c}{\lambda}\right)\frac{c}{\lambda^2} d\lambda, \tag{6}$$

where ν is the light frequency and $g_{vJ,v'J'}(\nu)$ the Lorentzian:

$$g_{vJ,v'J'}(\nu) = \pi \frac{\Delta\nu/2}{(\nu - \nu_{vv',JJ'})^2 + (\Delta\nu/2)^2}. \tag{7}$$

For collision and resonance broadening [22],

$$\Delta\nu = \sigma_0 v_0 n/\pi + 50\frac{n_{\mathrm{OH}} f_a}{\nu_{v'v'',J'J''}}, \tag{8}$$

where σ_0 is the collision cross section, v_0 the mean relative speed of molecules, n the number density of all particles, n_{OH} the number density of OH, and f_a the absorption oscillator strength. We simply use the diameters of the molecules to calculate the cross sections.

Suppose that the thermal excitation dominates the formation of the excited Na atoms in the process of SBSL; then, the calculation of the sodium line will be much simpler due to the absence of the vibrational and rotational structures, and the power of radiation of the line near 589 nm may be evaluated approximately by

$$P_{10} \approx \frac{n g_1 e^{-\Delta E/kT}}{1 + g_1 e^{-\Delta E/kT}} A_{10} h\nu_{10}, \tag{9}$$

where n is the number density of Na atoms inside the bubble, g_1 the Lande factor of 6, and ΔE the energy of the excited level relative to the ground state, and since the lifetime of Na atom at this excited level is $\tau = 1.66 \times 10^{-8}$ s, then $A_{10} = \frac{1}{\tau}$ [22]. Here other excited states of Na atoms are ignored. Considering the collision and resonance broadening, similar to Eq. (6), the radiation power per unit volume per unit wavelength interval for this sodium line is

$$P_\lambda d\lambda = P_{10} g_{10}\left(\nu = \frac{c}{\lambda}\right)\frac{c}{\lambda^2} d\lambda. \tag{10}$$

Here we should mention that those experimental data of the spectral radiation power reported in Refs. [4,6] are the average power per sound wave period—i.e., the average of $P(\lambda,t)$ in Eq. (3) during a sound wave period of $2\pi/\omega$,

$$\bar{P}(\lambda) = \frac{\omega}{2\pi}\int_0^{2\pi/\omega} P(\lambda,t) dt, \tag{11}$$

and the total radiation power is the integral over λ,

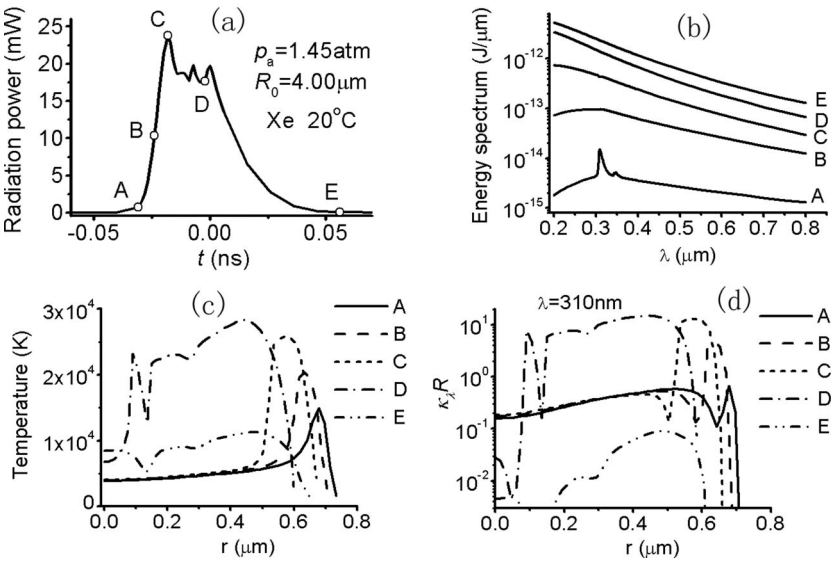

FIG. 2. A Xe bubble in 20 °C water for case *a* in Fig. 1. (a) Radiation power of the bubble vs time and for those several moments marked from *A* to *E*, (b) energy spectrum, (c) temperatures, and (d) absorption coefficient κ_λ at λ=310 nm times the bubble radius *R*, respectively.

$$P(t) = \int_{200\ \mathrm{nm}}^{800\ \mathrm{nm}} P(\lambda,t)d\lambda. \tag{12}$$

More precisely, we can evaluate the cumulate radiation energy emitted from a SBSL bubble from 0 to *t* within a sound wave period:

$$E_\lambda(t) = \int_0^t P(\lambda,t')dt', \quad 0 \leqslant t \leqslant \frac{2\pi}{\omega}. \tag{13}$$

Since the duration of light emission from a SBSL bubble is only a few hundred picoseconds, only during that short duration does $P(\lambda,t)$ not vanish; therefore, within a sound wave period, $E_\lambda(t)$ is zero before that light emission duration and keeps nonvanishing during that short duration. After that duration, $E_\lambda(t)$ will not change with time and it equals $2\frac{\pi}{\omega}\bar{P}(\lambda)$.

RESULTS AND DISCUSSION

With the formulas above, we calculate the OH line emission on a continuous spectral background. We consider Xe and Ar bubbles in 0 or 20 °C water with a driving acoustic wave frequency of 31.9 or 33.8 kHz, respectively, according to the cases of five different parameters: $(R_0,p_a) \Rightarrow$(4.0 μm, 1.45 atm), (4.0 μm, 1.36 atm), (4.0 μm, 1.32 atm), (4.0 μm, 1.25 atm), and (4.0 μm, 1.22 atm). In order to understand the calculated results more clearly, we mark those calculation cases in R_0-p_a parameter space where the curves of diffusive equilibrium are plotted; see points *a*, *b*, *c*, *d*, and *e* in Fig. 1.

First, we calculate a Xe bubble in 20 °C water for case *a* in Fig. 1. When the bubble is being compressed, it starts to heat up the inner gas and burst into flashing. With Eq. (12), we evaluate the radiation pulse per flash [see Fig. 2(a)]. Then, we are allowed to select several moments during the flash—i.e., points *A*, *B*, *C*, *D*, and *E*—to evaluate the time-dependent radiation energy spectrum with Eq. (13) [see Fig.

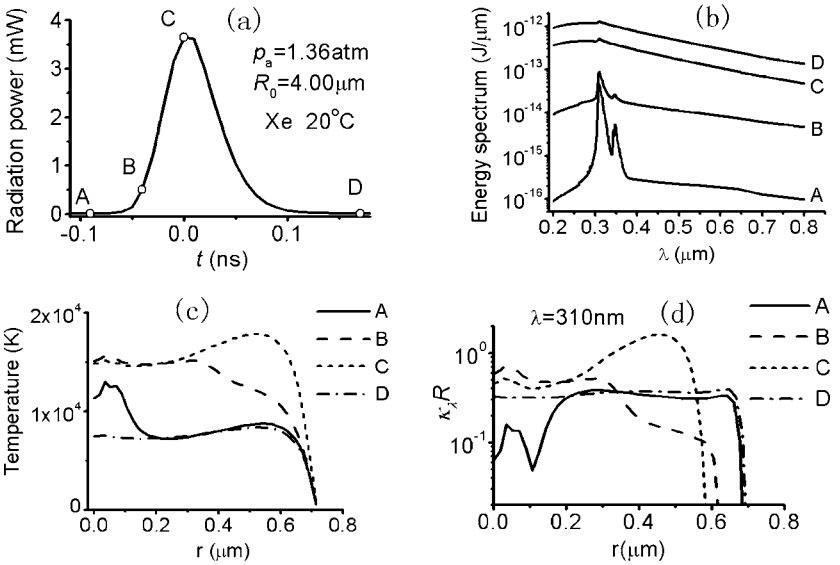

FIG. 3. The same as Fig. 2, but for case *b* in Fig. 1.

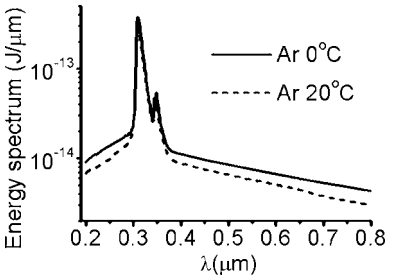

FIG. 4. Radiation energy spectra of the Ar bubble in 0 and 20 °C water for case *e* in Fig. 1.

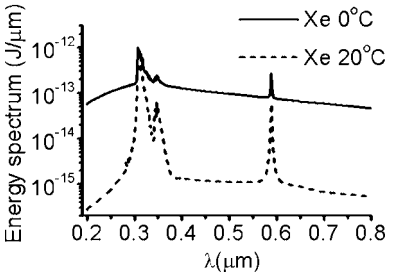

FIG. 5. Radiation energy spectra of the Xe bubble in 0 and 20 °C sodium sulfate solution for case *d* in Fig. 1.

2(b)] and corresponding temperatures [see Fig. 2(c)], respectively. Figure 2(d) shows the calculation of the absorption coefficient κ_λ at $\lambda=310$ nm times the bubble radius R. Roughly, if $\kappa_\lambda R \gg 1$, it means the bubble is opaque; if $\kappa_\lambda R \ll 1$, then it is transparent. If the bubble is opaque, then spectral lines should be absent and the spectrum should be featureless. As the radiation power increases from *A* to *C* [see Fig. 2(a)], the prominence of the OH line near 310 nm in the energy spectrum at *A* quickly merges into the background of the continuum spectrum and vanishes at *C* [see Fig. 2(b)]. This is because there is imploding shock formation at *B* which heats up the gas to form a high-temperature shell inside the bubble. At *C*, since the temperature of the shell is about 25 000 K [see Fig. 2(c)] and $\kappa_\lambda R \sim 10$ for $\lambda=310$ nm accordingly [see Fig. 2(d)], the bubble is opaque then. On the other hand, when the imploding shock wave is converging to the bubble center, the amount of molecules or atoms with high temperature changes, which results in the zigzag curve at the top of the pulse [see Fig. 2(a)]. At *E*, the light goes out, and the corresponding energy spectrum divided by the sound wave period is just the experimentally observed radiation power without the OH line on it.

If we lower the driving acoustic pressure, then the temperature inside the bubble may not be high enough to make the bubble opaque; in these cases, the results are a little different—for example, a Xe bubble in 20 °C water for case *b* in Fig. 1. Similar to Fig. 2, the results are illustrated in Fig. 3. As the radiation power increases from *A* to *C* [see Fig. 3(a)] the continuum emission processes gradually overwhelm the atomic or molecular line emission processes [9]; therefore, the prominence of the OH line near 310 nm in the energy spectrum at *A* and *B* gradually merges into the background of the continuum spectrum. However, this spectral line does not vanish out of the spectrum at *C* and *D*, and there remains a small visible bulge at 310 nm [see Fig. 3(b)]. It may be too small to be observed in experiments. At *C*, since the highest temperature is about 17 000 K [see Fig. 3(c)], $\kappa_\lambda R \sim 1$ for $\lambda=310$ nm [see Fig. 3(d)], the bubble is neither opaque nor transparent. In addition, since there is no shock formation inside the bubble, the top of the pulse is a smooth convex curve now [see Fig. 3(a)].

If we lower the driving acoustic pressure again, what is going to happen? According to the observations [6,7], the prominence of the OH line near 310 nm on the SBSL spectrum takes place when SBSL bubbles are unstable or dim under lower driving acoustic pressure—i.e., smaller p_a. In order to interpret this experimental result, we calculate the Ar bubble in 0 and 20 °C water for case *e* in Fig. 1, and the radiation energy spectra are plotted in Fig. 4. The prominence of the OH line near 310 nm is certain enough, and their broadenings are attributed to the contribution from the vibrational and rotational bands and the collision between molecules and atoms. Compared to Fig. 2 or 3, the light emissions from these two bubbles are much weaker than

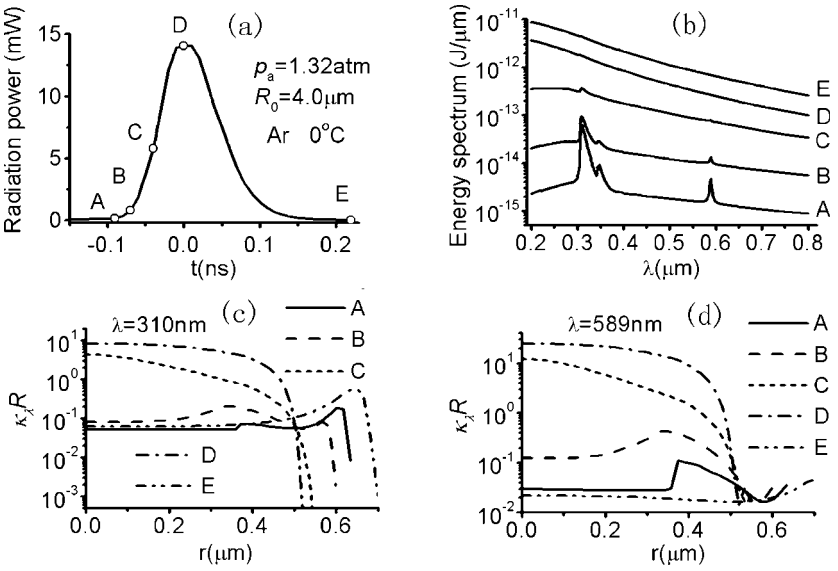

FIG. 6. An Ar bubble in 20 °C sodium sulfate solution for case *c* in Fig. 1. (a) Radiation power of the bubble vs time, (b) the evolution of the energy spectrum with moments marked from *A* to *E*, and (c), (d) the corresponding absorption coefficient κ_λ times the bubble radius R, for $\lambda=310$ and 589 nm, respectively.

bubbles in both Figs. 2 and 3. In addition, due to the vapor effects, the maximum temperature of the bubble in 0 °C water is about 13 900 K, while in 20 °C water it is about 11 300 K, and accordingly, the former bubble is slightly brighter.

If the bubble is not in pure water—for instance, in sodium sulfate solution—then the sodium line near 589 nm may appear on the SBSL spectrum [7], too. However, the mechanism for the formation of the excited Na atoms and the site where those emission lines originate are still under debate [24]. To obtain a sketchy quantitative evaluation of the sodium line on the SBSL spectrum, in the present calculation, we simply assume that the sodium line originates from those thermally excited Na atoms in the gas phase and set the number density of Na atoms inside the bubble n in Eq. (9) as 10^{-6} of n_{total}, the total number density of particles inside the bubble. As an example, we calculate the Xe bubble in 0 and 20 °C sodium sulfate solution for case d in Fig. 1. For simplicity, we treat sodium sulfate solution just as water in the calculation. Although it is assumed that there is a very small amount of Na atoms of $10^{-6}n_{\text{total}}$ inside the bubble, the apparent prominence of the sodium line near 589 nm, in addition to the OH line, in 0 and 20 °C environment is shown in Fig. 5. On the other hand, due to the vapor effects, the maximum temperature of the Xe bubble in 0 °C environment is about 13 000 K, while in 20 °C environment it is only about 8 000 K, which makes the former bubble much brighter than the latter.

To further understand the process of the prominence or absence of spectral lines, we give another example, an Ar bubble in 20 °C sodium sulfate solution for case c in Fig. 1. Similar to the case in Fig. 2, we calculate the light emission pulse [see Fig. 6(a)] and mark moments A, B, C, D, and E on the curve. One can see in the process how the OH line near 310 nm and the sodium line near 589 nm gradually change from prominence to absence, as the radiation is gradually strengthening [see curves $A-D$ in Fig. 6(b)]. Figures 6(c) and 6(d) show the calculation of the absorption coefficient κ_λ times the bubble radius R. As Figs. 6(c) and 6(d) show, for A, B, and E, the bubble is transparent for both $\lambda=310$ and 589, while for D, it is certainly opaque, which leads to the disappearance of the atomic or molecular line in the SBSL spectrum.

With the present model, we can also evaluate the light emission energies that different processes contribute. For the sake of simplicity, processes of electron-neutral atom bremsstrahlung, electron-ion bremsstrahlung, and recombination radiation altogether are labeled as process 1, processes of the radiative attachment of electrons to atoms and molecules as process 2, and processes of OH line emission as process 3. Table I lists the percentages of light emission energies that those three defined processes contribute. The last column lists the total light emission energies for different cases. We find that process 1 contributes most of the radiation energy to those bright SBSL bubbles, and we declare here that the calculation in Ref. [10] overestimated the contribution of process 2. For some SBSL bubbles with a distinct appearance of the OH line spectrum, the molecular line emission process contributes most of the radiation energy.

TABLE I. The percentages of light emission energies different processes contribute and the total light emission energies for different cases.

	Process 1	Process 2	Process 3	Total radiation energy (J)
Case *a* Xe 20 °C	99.73%	0.24%	0.03%	7.27×10^{-13}
Case *b* Xe 20 °C	95.88%	3.58%	0.54%	3.46×10^{-13}
Case *c* Xe 0 °C	98.26%	1.54%	0.20%	3.16×10^{-12}
Case *c* Ar 0 °C	97.85%	1.79%	0.36%	1.32×10^{-12}
Case *d* Xe 0 °C	73.38%	11.81%	14.81%	6.69×10^{-14}
Case *d* Xe 20 °C	2.27%	5.01%	92.72%	7.01×10^{-15}
Case *d* Ar 0 °C	85.23%	10.15%	4.62%	1.40×10^{-13}
Case *d* Ar 20 °C	82.45%	13.29%	4.26%	7.48×10^{-14}
Case *e* Ar 0 °C	37.05%	13.06%	49.89%	1.08×10^{-14}
Case *e* Ar 20 °C	25.06%	22.38%	52.56%	8.61×10^{-15}

CONCLUSION

According to the present calculation, the maximum temperature of the SBSL bubble determines whether the spectral lines appear or disappear on the spectrum. The prominence of the OH line near 310 nm or the sodium line near 589 nm implies that the maximum temperature is not high enough for the spectral line emission processes to be comparable or overwhelm the processes of continuous emission. For those bright SBSL bubbles, the spectral lines are absent because of the following two reasons: first, the processes of continuous emission overwhelm the spectral line emission processes [9]; second, the maximum temperature makes the bubble opaque for a wavelength corresponding to the spectral line. In general, the prominence of the molecular spectral line in the SBSL spectrum means a lower maximum temperature than that in the absence case. On the other hand, although we do not know whether a similar mechanism makes the spectral lines of inert gas atoms disappear for the SBSL bubble in water, but appear in sulfuric acid [25], the analysis of atomic lines in the SBSL spectrum may provide more reliable information about the maximum temperature inside the bubble.

ACKNOWLEDGMENT

This work is supported by the NSFC under Grants No. 10674081 and 10434070.

[1] H. Frenzel and H. Schultes, Z. Phys. Chem. Abt. B **27**, 421 (1934).
[2] D. F. Gaitan, L. A. Crum, C. C. Church, and R. Roy, J. Acoust. Soc. Am. **91**, 3166 (1992).
[3] B. P. Barber and S. J. Putterman, Nature (London) **352**, 318 (1991).
[4] B. P. Barber *et al.*, Phys. Rep. **281**, 65 (1997).
[5] T. J. Matula, R. A. Roy, P. D. Mourad, W. B. McNamara III, and K. S. Suslick, Phys. Rev. Lett. **75**, 2602 (1995).
[6] J. B. Young, J. A. Nelson, and W. Kang, Phys. Rev. Lett. **86**, 2673 (2001).
[7] J. F. Xu, W. Z. Chen, X. H. Xu, Y. Liang, and W. Huang, Phys. Rev. E **76**, 026308 (2007).
[8] S. Hilgenfeldt, D. Lohse, and M. Brenner, Phys. Fluids **8**, 2808 (1996); **9**, 2462(E) (1996).
[9] M. P. Brenner, S. Hilgenfeldt, and D. Lohse, Rev. Mod. Phys. **74**, 425 (2002).
[10] Yu An, Phys. Rev. E **74**, 026304 (2006).
[11] L. D. Landau and E. M. Lifshitz, *Statistical Physics*, 2nd ed. (Pergamon Press, New York, 1980).
[12] D. Lohse, M. P. Brenner, T. F. Dupont, S. Hilgenfeldt, and B. Johnston, Phys. Rev. Lett. **78**, 1359 (1997).
[13] S. Geltman, J. Quant. Spectrosc. Radiat. Transf. **13**, 601 (1973).
[14] S. Hilgenfeldt, S. Grossmann, and D. Lohse, Nature (London) **398**, 402 (1999).
[15] K. Yasui, Phys. Rev. E **64**, 016310 (2001).
[16] D. Hammer and L. Frommhold, Phys. Rev. E **65**, 046309 (2002).
[17] Yu An and C. F. Ying, Phys. Rev. E **71**, 036308 (2005).
[18] L. Rayleigh, Philos. Mag. **34**, 94 (1917); M. Plesset, J. Appl. Mech. **16**, 277 (1949); B. Noltingk and E. Neppiras, Proc. Phys. Soc. London, Sect. B **63**, 674 (1950); J. B. Keller and I. I. Kolodner, J. Appl. Phys. **27**, 1152 (1956).
[19] L. S. Bernstein, M. R. Zakin, E. B. Flint *et al.*, J. Phys. Chem. **100**, 6612 (1996).
[20] G. Herzberg, *Spectra of Diatomic Molecules*, Vol. 1 of *Molecular Spectra and Molecular Structure* (Van Nostrand Reinhold, New York, 1950), pp. 107, 208, and 382.
[21] T. Carrington, J. Chem. Phys. **30**, 1087 (1959).
[22] R. Mavrodineanu and H. Boiteux, *Flame Spectroscopy* (John Wiley & Sons, Inc., New York, 1965), pp. 41 and 516.
[23] K. R. Lang, *Astrophysical Formulae: A Compendium for the Physicist and Astrophysicist* (Springer, Berlin, 1974), pp. 211–217.
[24] D. Sunartio, K. Yasui, T. Tuziuti *et al.*, ChemPhysChem **8**, 2331 (2007).
[25] D. J. Flannigan and K. S. Suslick, Nature (London) **434**, 52 (2005).